Radical−Molecule Reactions HCO/HOC + C_2H_2: Mechanistic Study

Hao Dong, Yi-hong Ding,* and Chia-chung Sun

State Key Laboratory of Theoretical and Computational Chemistry, Institute of Theoretical Chemistry, Jilin University, Changchun 130023, People's Republic of China

Received: December 15, 2004; In Final Form: March 3, 2005

A detailed computational study is performed on the unknown radical−molecule reactions between HCO/HOC and acetylene (C_2H_2) at the CCSD(T)/6-311G(2d,p)//B3LYP/6-311G(d,p)+ZPVE, Gaussian-3//B3LYP/6-31G(d), and Gaussian-3//MP2(full)/6-31G(d) levels. For the HCO + C_2H_2 reaction, the most favorable pathway is direct C-addition forming the intermediate HC═CHCH═O followed by a 1,3-H-shift leading to H_2C═CHC═O, which finally dissociates to the product C_2H_3 + CO. The overall reaction barrier is 13.8, 10.5, and 11.3 kcal/mol, respectively, at the three levels. The quasi-direct H-donation process to produce C_2H_3 + CO with barriers of 14.0, 14.1, and 14.1 kcal/mol is less competitive. Thus only at higher temperatures could the HCO + C_2H_2 reaction play a role. In contrast, the HOC + C_2H_2 reaction can barrierlessly generate C_2H_3 + CO via the quasi-direct H-donation mechanism proceeding via a prereactive complex with OH···C_2 hydrogen bonding. This is suggestive of the potential importance of the HOC + C_2H_2 reaction in both combustion and interstellar processes. However, the direct C-addition channel is much less competitive. For both reactions, the possible formation of the intriguing interstellar molecules propadiene and propynal is also discussed. The present theoretical study represents the first attempt to probe the reaction mechanism between HOC and π-systems. Future laboratory investigations on both reactions (particularly HOC + C_2H_2) are recommended.

1. Introduction

The formaldehyde radical (H•C═O) has been considered to play an important role in various fields including combustion chemistry, photochemistry, stratospheric chemistry, and astrophysical chemistry.[1,2] Accordingly, it has been the subject of a large number of experimental and theoretical investigations.[1−37] While its structural, spectroscopic, and dissociation properties are well-known,[1−16] its reactions, such as those with H,[16,17] Cl,[18] OH,[17] HBr, HI,[19] O_2,[20−27] NO,[17,20,24,28] Cl_2,[21,24] Br_2,[21,29] HCO,[16] HCN,[30] HNO,[31] NO_2,[17,21,24,32−34] HNCO,[35] HNOH, HONO,[36] CH_3, C_2H_5, *n*-C_3H_7, *i*-C_3H_7, and *t*-C_4H_9,[37] have also been studied extensively. However, to our surprise, the HCO reaction with acetylene (C_2H_2) has never been considered before, though both reactants may coexist. Acetylene is an archetype of C≡C triple bonding for hydrocarbons. To what degree this reaction can take place is still uncertain. The possibility of the HCO + C_2H_2 reaction in space is also of interest because both species have been detected. Moreover, the intriguing interstellar molecule propynal (HC≡CCH═O) and propadiene (H_2C═C═C═O) are formally related to this reaction. We wonder whether either of them or both can be favorably formed via this reaction. Thus, it is desirable to explore the mechanism of the HCO + C_2H_2 reaction both qualitatively and quantitatively, as will be reported in section 3.1.

In sharp contrast to the rich knowledge of HCO, the isomeric form HOC has received rather little attention from only several papers, possibly due to its calculated high energy and lack of experimental data.[1,3,4,11] The very recent high-level theoretical study[11] found that despite the high energy, the HOC radical has considerable barriers toward isomerization and dissociation. Once generated, HOC could have a certain lifetime of existence, at least as a transient species. In circumstances with very low temperatures such as dense interstellar clouds (T < 100 K), the existence of HOC is very promising. The intrinsic stability of HOC thus leads us to consider that the experimental detection of HOC seems to be just a matter of time, as was stated in the same paper.[11] The HOC radical could be one possible intermediate in various gas-phase processes. In interstellar space, the reaction between the abundant atomic hydrogen and carbon

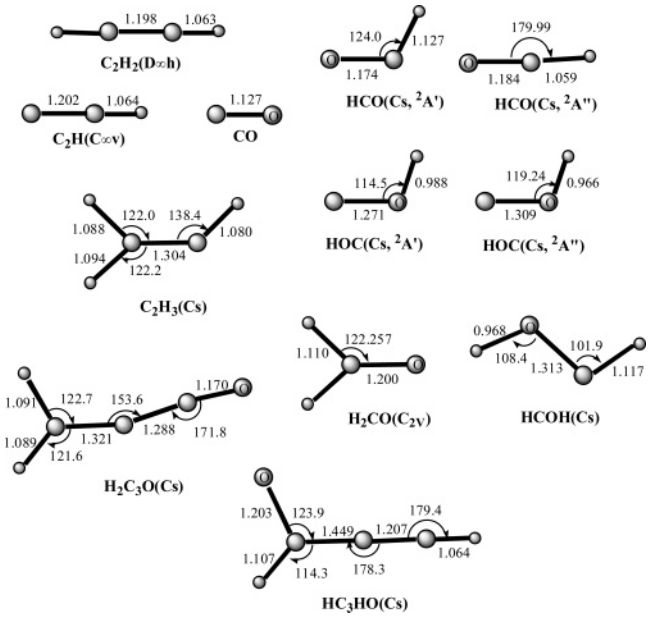

Figure 1. Optimized structures of reactants and products at B3LYP/6-311G(d,p) levels. Bond lengths are in angstroms and angles are in degrees.

* Corresponding author. E-mail: yhdd@mail.jlu.edu.cn.

10.1021/jp0442854 CCC: $30.25
Published on Web 12/06/2005

TABLE 1: Zero-Point Vibrational Energies (kcal/mol) and Total Energies (au), with Relative Energies in Parentheses (kcal/mol), of Reactants, Products, and Isomers at B3LYP/6-311G(d,p) Level and CCSD(T)/6-311G(2d,p)//B3LYP/6-311G(d,p)+ZPVE Level

species	ZPVE	B3LYP	CCSD(T)	CCSD(T)+ZPVE
R$_1$ C_2H_2 + HCO	0.039904	−191.2412930 (0.0)	−190.7932789 (0.0)	0.0
R$_2$ C_2H_2 + HOC	0.040152	−191.1743069 (42.0)	−190.7269270 (41.6)	41.8
P$_1$ C_2H_3 + CO	0.041393	−191.2732679 (−20.1)	−190.8324750 (−24.6)	−23.7
P$_2$ H_2C_3O + H	0.037260	−191.2150322 (16.5)	−190.7598899 (21.0)	19.3
P$_3$ HC_3HO + H	0.037138	−191.2045339 (23.1)	−190.7584293 (21.9)	20.1
P$_4$ C_2H + H_2CO	0.040957	−191.1657999 (47.4)	−190.7234594 (43.8)	44.5
P$_5$ HCOH + C_2H	0.041219	−191.081563 (100.2)	−190.640272 (96.0)	96.8
Com1	0.041268	−191.2444386 (−2.0)	−190.797173 (−2.4)	−1.6
Com2	0.042423	−191.1828553 (36.7)	−190.7358513 (36.0)	37.6
1a	0.048784	−191.316237 (−47.0)	−190.8637931 (−44.2)	−38.7
1b	0.047212	−191.319381 (−49.0)	−190.8597332 (−41.7)	−37.1
2	0.047330	−191.305725 (−40.4)	−190.8442707 (−32.0)	−27.3
3a	0.046577	−191.289037 (−30.0)	−190.8294676 (−22.7)	−18.5
3b	0.046642	−191.279650 (−24.1)	−190.8253710 (−20.1)	−15.9
4a	0.047108	−191.279936 (−24.2)	−190.8269717 (−21.1)	−16.6
4b	0.047297	−191.279795 (−24.2)	−190.8268538 (−21.0)	−16.4
4c	0.047273	−191.276905 (−22.3)	−190.8239328 (−19.2)	−14.6
4d	0.047002	−191.274757 (−21.0)	−190.8217756 (−17.9)	−13.4
5a	0.047229	−191.280367 (−24.5)	−190.8219960 (−18.0)	−13.4
5b	0.046873	−191.276520 (−22.1)	−190.8184759 (−15.8)	−11.4
6	0.046166	−191.268841 (−17.3)	−190.8084810 (−9.5)	−5.6
7	0.046247	−191.244002 (−1.7)	−190.7914714 (1.1)	5.1
8a	0.048726	−191.213085 (17.7)	−190.7580520 (22.1)	27.6
8b	0.045609	−191.200419 (25.6)	−190.7462489 (29.5)	33.1
8c	0.047857	−191.208391 (20.6)	−190.7535479 (24.9)	29.9
8d	0.045358	−191.199794 (26.0)	−190.7451426 (30.2)	33.6
8e	0.047562	−191.206550 (21.8)	−190.7513186 (26.3)	31.1
8f	0.045166	−191.200689 (25.5)	−190.7458711 (29.7)	33.1
9a	0.047293	−191.198046 (27.2)	−190.7438775 (31.0)	35.6
9b	0.046847	−191.193700 (29.9)	−190.7406107 (33.0)	37.4
9c	0.046419	−191.194797 (29.2)	−190.7408271 (33.0)	37.0
9d	0.046058	−191.192406 (30.7)	−190.7393869 (33.8)	37.7
9e	0.047097	−191.199502 (26.2)	−190.7480673 (28.4)	32.9
9f	0.046866	−191.197888 (27.2)	−190.7463019 (29.5)	33.8
9g	0.045965	−191.193273 (30.1)	−190.7415873 (32.4)	36.2
9h	0.045659	−191.191237 (31.4)	−190.7394581 (33.8)	37.4
10	0.043467	−191.168614 (45.6)	−190.7172371 (47.7)	50.0
11	0.045398	−191.165811 (47.4)	−190.7153349 (48.9)	52.4
12	0.044286	−191.149839 (57.4)	−190.686932 (66.7)	69.5
13a	0.047106	−191.198322 (27.0)	−190.7450501 (30.3)	34.8
13b	0.046797	−191.194953 (29.1)	−190.7417947 (32.3)	36.6
14a	0.047771	−191.233721 (4.8)	−190.7756953 (11.0)	16.0
14b	0.047767	−191.233041 (5.2)	−190.7749789 (11.5)	16.4
14c	0.047818	−191.227770 (8.5)	−190.7713050 (13.8)	18.8
15	0.046099	−191.239469 (1.1)	−190.7815907 (7.4)	11.2
16a	0.048387	−191.222927 (11.5)	−190.7690932 (15.2)	20.5
16b	0.048056	−191.218178 (14.5)	−190.7641442 (18.3)	23.4
17	0.048030	−191.207397 (21.3)	−190.7535627 (24.9)	30.0
18	0.047469	−191.243430 (−1.3)	−190.7863964 (4.3)	9.1
19	0.047543	−191.227520 (8.6)	−190.7719266 (13.4)	18.2
20	0.046947	−191.222002 (12.1)	−190.7709052 (14.0)	18.5
21	0.047751	−191.260773 (−12.2)	−190.8051063 (−7.4)	−2.5
22	0.049687	−191.226730 (9.1)	−190.7759063 (10.9)	17.0
23a	0.047431	−191.198203 (27.0)	−190.7435784 (31.2)	35.9
23b	0.046180	−191.188379 (33.2)	−190.7332037 (37.7)	41.6

monoxide (CO) molecule can probably generate HOC as well as the HCO radical. The present failure of the HOC detection in laboratories may be ascribed to its high reactivity with other stable molecules. Therefore, knowledge of the HOC reactions is of significance to understanding its intermolecular stability and depletion rate in combustion and interstellar processes. Unfortunately, to the best of our knowledge, HOC reactions have not been the subject of previous investigations both theoretically and experimentally. In this paper, the HOC + C_2H_2 reaction mechanism is theoretically explored for the first time, as described in section 3.2. The implications of both the HCO/HOC + C_2H_2 reactions in combustion and astrophysical chemistry are discussed in section 3.3.

2. Computational Methods

All the calculations were carried out using the Gaussian 98 program package.[38] The geometries of stationary points including minimum isomers, transition states, and dissociated products were initially optimized at the B3LYP/6-311G(d,p) level followed by single-point CCSD(T)/6-311G(2d,p) calculations to obtain an overall picture about the reactions. The stationary nature of various structures was confirmed by the B3LYP/6-311G(d,p) harmonic vibrational frequency calculations. Minimum isomers possess all real frequencies, whereas transition states possess one and only one imaginary frequency. To test whether the obtained transition states connect the right isomers, intrinsic reaction coordinate (IRC) calculations were performed

TABLE 2: Zero-Point Vibrational Energies (kcal/mol) and Total Energies (au), with Relative Energies in Parentheses (kcal/mol), of Transition States at B3LYP/6-311G(d,p) Level and CCSD(T)/6-311G(2d,p)//B3LYP/6-311G(d,p)+ZPVE Level

TS	ZPVE	B3LYP	CCSD(T)	CCSD(T)+ZPVE
TSCom1/P_1	0.037556	−191.2247204 (10.4)	−190.768619 (15.5)	14.0
TSCom2/P_1	0.03851	−191.1798032 (38.6)	−190.7265545 (41.9)	41.0
TSCom2/P_1*	0.037581	−191.1747042 (41.8)	−190.7192804 (46.4)	45.0
TSR_1/4b	0.042117	−191.2322668 (5.7)	−190.7787864 (9.1)	10.5
TSR_1/7a	0.040943	−191.1745298 (41.9)	−190.7165758 (48.1)	48.8
TSR_1/11	0.042456	−191.1605685 (50.7)	−190.704161 (55.9)	57.5
TSR_1/P_4	0.041277	−191.1683881 (45.7)	−190.7243533 (43.3)	44.1
TSR_2/9a	0.041952	−191.1575376 (52.6)	−190.7063559 (54.5)	55.8
TSR_2/9a*	0.042246	−191.1582793 (52.1)	−190.7042528 (55.9)	57.3
TS1a/1b	0.047091	−191.3122095 (−44.5)	−190.8574075 (−40.2)	−35.7
TS1b/2	0.043367	−191.243638 (−1.5)	−190.776785 (10.4)	12.5
TS1b/3a	0.042444	−191.242190 (−0.6)	−190.775075 (11.4)	13.0
TS1a/4a	0.042897	−191.230988 (6.5)	−190.774215 (12.0)	13.8
TS1a/14c	0.045044	−191.172456 (43.2)	−190.713653 (50.0)	53.2
TS1b/17	0.041848	−191.115059 (79.2)	−190.659136 (84.2)	85.4
TS1a/P_1	0.042943	−191.2725436 (−19.6)	−190.828726 (−22.2)	−20.3
TS2/17	0.040170	−191.122107 (74.8)	−190.666831 (79.3)	79.5
TS2/20	0.045339	−191.205054 (22.7)	−190.753832 (24.8)	28.2
TS3a/3b	0.046293	−191.2795385 (−24.0)	−190.8248807 (−19.8)	−15.8
TS3a/4b	0.040931	−191.2046777 (23.0)	−190.7438034 (31.0)	31.7
TS3a/4c	0.040965	−191.204050 (24.4)	−190.743979 (30.9)	31.6
TS3b/5a	0.043456	−191.205645 (23.4)	−190.749222 (27.6)	29.9
TS3a/18	0.044799	−191.230899 (6.5)	−190.767757 (16.0)	19.1
TS3b/P_2	0.038617	−191.2137089 (17.3)	−190.7566555 (23.0)	22.2
TS3a/P_3	0.037845	−191.2030785 (24.0)	−190.7522864 (25.7)	24.4
TS4a/4b	0.045489	−191.273732 (−20.4)	−190.818845 (−16.0)	−12.5
TS4b/4c	0.046180	−191.268373 (−17.0)	−190.817540 (−15.2)	−11.3
TS4c/4d	0.045392	−191.269218 (−17.5)	−190.814275 (−13.2)	−9.7
TS4b/5a	0.040371	−191.1797898 (38.6)	−190.718484 (47.0)	47.2
TS4a/7	0.040676	−191.201970 (24.7)	−190.740321 (33.2)	33.7
TS4c/8a	0.044558	−191.206813 (21.6)	−190.751142 (26.4)	29.4
TS4c/9a	0.041266	−191.145585 (60.1)	−190.690420 (64.5)	65.4
TS4d/9b	0.040876	−191.140600 (63.2)	−190.686591 (67.0)	67.6
TS4d/15	0.044975	−191.238168 (2.0)	−190.780254 (8.2)	11.4
TS4c/21	0.046086	−191.214112 (17.1)	−190.758058 (22.1)	26.0
TS4a/P_3	0.038151	−191.2010533 (25.3)	−190.7504589 (26.9)	25.8
TS5a/5b	0.045759	−191.269700 (−17.8)	−190.812318 (−11.9)	−8.3
TS5b/7	0.042443	−191.199822 (26.0)	−190.742190 (32.1)	33.7
TS5a/8d	0.042854	−191.196507 (28.1)	−190.741885 (32.3)	34.1
TS5b/8f	0.042346	−191.197299 (27.6)	−190.742566 (31.8)	33.4
TS5a/9h	0.040563	−191.153480 (55.1)	−190.692900 (63.0)	63.4
TS5a/16a	0.046806	−191.205481 (22.5)	−190.749808 (27.3)	31.6
TS5a/P_3	0.03805	−191.1991953 (26.4)	−190.7430189 (31.5)	30.7
TS6/9c	0.041147	−191.139014 (64.2)	−190.676484 (73.3)	74.1
TS6/16a	0.041982	−191.136824 (65.6)	−190.682172 (69.7)	71.0
TS6/16b	0.041953	−191.133944 (67.4)	−190.679129 (71.6)	72.9
TS6/17	0.045786	−191.1997914 (26.0)	−190.7451139 (30.2)	33.9
TS7a/P_3	0.038486	−191.1985287 (26.8)	−190.7463351 (29.5)	28.6
TS8a/8b	0.044337	−191.193976 (29.7)	−190.740444 (33.2)	35.9
TS8c/8e	0.045200	−191.193752 (29.8)	−190.739402 (33.8)	37.1
TS8d/8f	0.044005	−191.1937091 (29.9)	−190.7397143 (33.6)	36.2
TS8b/10	0.040307	−191.123743 (73.8)	−190.668896 (78.1)	78.3
TS8c/14c	0.043557	−191.166952 (46.6)	−190.713700 (49.9)	52.2
TS8e/14c	0.043985	−191.170874 (44.2)	−190.717266 (47.7)	50.3
TS8a/16a	0.046717	−191.202617 (24.3)	−190.747755 (28.6)	32.8
TS8e/16b	0.046375	−191.204151 (23.3)	−190.749993 (27.1)	31.2
TS8b/22	0.042167	−191.123220 (74.1)	−190.669065 (77.9)	79.4
TS9a/9b	0.045258	−191.1883043 (33.3)	−190.7329789 (37.8)	41.2
TS9a/9c	0.044123	−191.165514 (47.6)	−190.706880 (54.2)	56.9
TS9a/9e	0.045906	−191.1899369 (32.2)	−190.737882 (34.8)	38.5
TS9b/9d	0.043985	−191.160348 (50.8)	−190.703698 (56.2)	58.8
TS9b/9f	0.045715	−191.1877068 (33.6)	−190.7364273 (35.7)	39.3
TS9c/9d	0.044495	−191.1877711 (33.6)	−190.732586 (38.1)	41.0
TS9c/9g	0.045184	−191.1875099 (33.7)	−190.7353636 (36.3)	39.7
TS9d/9h	0.044893	−191.1847623 (35.4)	−190.7332451 (37.7)	40.8
TS9e/9f	0.045265	−191.1910211 (31.5)	−190.7376509 (34.9)	38.3
TS9e/9g	0.043541	−191.1625371 (49.4)	−190.704106 (56.0)	58.2
TS9f/9h	0.043622	−191.1614348 (50.1)	−190.703824 (56.1)	58.5
TS9g/9h	0.044035	−191.185278 (35.1)	−190.731633 (38.7)	41.3
TS9e/14c	0.045939	−191.186880 (34.1)	−190.729812 (39.8)	43.6
TS9f/14c	0.046225	−191.1880963 (33.4)	−190.7317581 (38.6)	42.6
TS9g/14c	0.045221	−191.180629 (38.1)	−190.723685 (43.7)	47.0
TS9h/14c	0.045309	−191.181313 (37.6)	−190.7249643 (42.9)	46.3

TABLE 2 (Continued)

TS	ZPVE	B3LYP	CCSD(T)	CCSD(T)+ZPVE
TS12/18	0.043786	−191.133846 (67.4)	−190.677448 (72.7)	75.1
TS13a/13b	0.045525	−191.186429 (34.4)	−190.733669 (37.4)	40.9
TS13b/14a	0.043488	−191.167442 (46.3)	−190.713948 (49.8)	52.0
TS13a/17	0.046707	−191.197972 (27.2)	−190.743795 (31.1)	35.3
TS13a/18	0.041481	−191.156018 (53.5)	−190.702774 (56.8)	57.8
TS14a/14b	0.046349	−191.2303867 (6.8)	−190.7722108 (13.2)	17.3
TS14b/14c	0.045665	−191.2122248 (18.2)	−190.7539818 (24.7)	28.3
TS14c/15	0.042063	−191.169132 (45.3)	−190.708959 (53.0)	54.3
TS14a/16b	0.040657	−191.126461 (72.1)	−190.669259 (77.8)	78.3
TS15/23b	0.045042	−191.184303 (35.8)	−190.727169 (41.5)	44.7
TS16a/16b	0.047150	−191.2131158 (17.7)	−190.7602363 (20.7)	25.3
TS18/19	0.038442	−191.062577 (112.1)	−190.603332 (119.2)	118.3
TS21/23a	0.046428	−191.193111 (30.2)	−190.739448 (33.8)	37.9
TS23a/23b	0.045183	−191.187253 (33.9)	−190.730908 (39.1)	42.5

TABLE 3: Zero-Point Vibrational Energies (kcal/mol) and Total Energies (au), with Relative Energies in Parentheses (kcal/mol), of R_1, R_2, Com1, Com2, and Some Key Transition States at Various Levels

species	ZPVE	B3LYP	CCSD(T)	CCSD(T)+ZPVE	G3B3	G3MP2
R_1 C_2H_2 + HCO	0.039904	−191.2412930	−190.7932789	−190.7533749 (0.0)	−191.072795 (0.0)	−190.915019 (0.0)
R_2 C_2H_2 + HOC	0.040152	−191.1743069	−190.7269270	−190.686775 (41.8)	−191.005965 (41.9)	−190.847629 (42.3)
Com1	0.041268	−191.2444386	−190.7971730	−190.755905 (−1.6)	−191.074461 (−1.0)	−190.917032 (−1.3)
Com2	0.042423	−191.1828553	−190.7358513	−190.6934283 (37.6)	−191.012296 (37.9)	−190.854587 (37.9)
TSCom1/P_1	0.037556	−191.2247204	−190.7686190	−190.731063 (14.0)	−191.050267 (14.1)	−190.892519 (14.1)
TSCom2/P_1	0.038510	−191.1798032	−190.7265545	−190.6880445 (41.0)	−191.008988 (40.0)	−190.8493462 (41.2)
TSCom2/P_1*	0.037581	−191.1747042	−190.7192804	−190.6816994 (45.0)	−191.002728 (43.9)	−190.843390 (45.0)
TSR_1/4b	0.042117	−191.2322668	−190.7787864	−190.7366694 (10.5)	−191.059450 (8.4)	−190.901025 (8.8)
TS1a/4a	0.042897	−191.2309876	−190.7742153	−190.7313183 (13.8)	−191.056110 (10.5)	−190.896955 (11.3)

at the B3LYP/6-311G(d,p) level. For the relevant entrance channels, the recently developed Gaussian-3//B3LYP/6-31G(d) and Gaussian-3//MP2(full)/6-31G(d) methods were applied to get more reliable energetic predictions. As a default in the Gaussian program, for species with odd electrons (such as HCO/COH), the unrestricted methods are used throughout for both geometric and single-point energy calculations. For those with even electrons (such as C_2H_2), the restricted methods are used.

3. Results and Discussion

Prior to the discussion, we would like to consider the possible electronic states of both HCO and HOC radicals. Each radical has two kinds of states, i.e., $^2A'$ and $^2A''$, for which the unpaired electron is in and perpendicular to the [H,C,O] plane, respectively. Their structural parameters are shown in Figure 1. For both radicals, the $^2A'$ state structure is bent. Yet, for the $^2A''$ state, HCO becomes linear, whereas HOC remains bent. Energetically, the $^2A''$ state is much less stable than the $^2A'$ state for both radicals; i.e., the energy difference is 26.24 and 20.84 kcal/mol, respectively, for HCO and HOC at the B3LYP/6-311G(d,p) level. Therefore, in the following discussions, HCO and HOC are both considered to have the ground state $^2A'$.

For the HCO/HOC + C_2H_2 reactions, the energetics of the intermediate isomers, reactants, and products are listed in Table 1, while those of the transition states are given in Table 2. In addition, Table 3 gives a comparison on the most relevant channels calculated at various levels. The total energy of the reactant **R_1** HCO + C_2H_2 is set to zero for reference. Figure 1 shows the optimized structures of the reactants and various dissociation products. Figures 2 and 3 depict the optimized structures of the isomers and transition states, respectively. Finally, the schematic potential energy surfaces (PESs) of the HCO + C_2H_2 and HOC + C_2H_2 reactions are illustrated in Figures 4 and 5, respectively. In the following discussions, we first analyze the possible isomerization and dissociation channels for each reaction at the CCSD(T)/6-311G(2d,p)//B3LYP/6-311G(d,p)+ZPVE level (simplified as CCSD(T)//B3LYP). Then, for the most competitive channels, we discuss the higher level Gaussian-3//B3LYP/6-31G(d) and Gaussian-3//MP2-(full)/6-31(d) results, which are simplified as G3//B3YP and G3//MP2, respectively. Generally, there are many transition states associated with the isomerization between various C_3H_3O isomers. For simplicity and easy discussion, for some less-important isomers, only the lowest or former low-lying transition states are indicated in Figures 4 and 5.

3.1. HCO + C_2H_2 Reaction. As shown in Figure 4, we identified five kinds of entrance channels: (1) direct H-abstraction channel forming **P_4** H_2CO + C_2H (44.5) via the transition state **TSR_1/P_4** (44.1); (2) quasi-direct H-donation channel forming **P_1** CO + C_2H_3 (−23.7) via **TSCom1/P_1** (14.0); (3) C-addition channel forming the intermediate HCCHCHO **4** [**4a** (−16.6), **4b** (−16.4), **4c** (−14.6) and **4d** (−13.4)] via **TSR_1/4b** (10.5), (4) O-addition channel forming HCOCHCH **11** (52.4) via **TSR_1/11** (57.5), and (5) concerted C-addition and 1,2-H-shift channel leading to $HCCCH_2O$ **7** (5.1) via **TSR_1/7** (48.8). The values in parentheses are CCSD(T)//B3LYP relative energies. The interconversion between the isomeric forms of **4** is easy. Surely, the direct H-abstraction channel (1) with the highest energy transition state is the least feasible since C_2H_2 is reluctant to lose H-atom due to its very large C−H bond energy.[39] Another H-abstraction product **P_5** HCOH + C_2H is not considered because it is already 96.8 kcal/mol higher in energy than **R_1**. The C-addition channel (3) and the H-donation channel (2) are the former two feasible pathways of interest.

The C-addition isomer HCCHCHO **4** can take nine evolution pathways, with increasing transition state energies: (1) **4d** → **15**, (2) **4a** → **1a**, (3) **4a** → **P_3**, (4) **4c** → **21**, (5) **4c** → **8a**, (6) **4b**/**4c** → **3a**, (7) **4a** → **7**, (8) **4b** → **5a**, and (9) **4c**/**4d** → **9a**/**9b**. We first exclude the contribution from channels 1 and 5 because the corresponding reverse conversions have very small barriers of just 0.2 and 1.8 kcal/mol. Thus, channel 2 is the most effective pathway of intermediate **4** leading to the lowest lying isomers H_2CCHCO **1a** (−38.7) and **1b** (−37.1) via 1,3-H-shift **TS1a/4a** (13.8). The second favorable pathway of **4**, i.e., channel

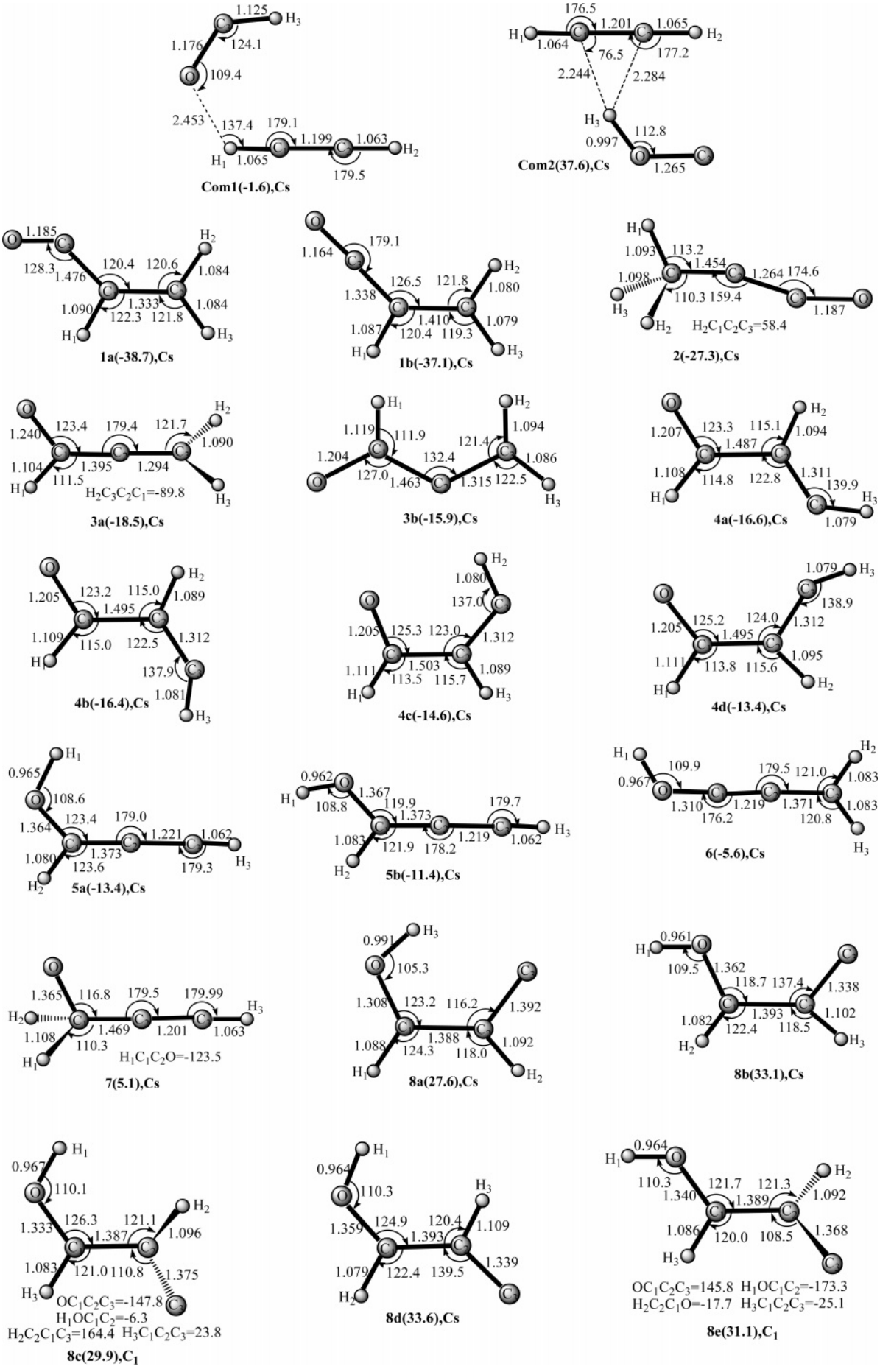
Com1(-1.6),Cs
Com2(37.6),Cs
1a(-38.7),Cs
1b(-37.1),Cs
2(-27.3),Cs
$H_2C_1C_2C_3$=58.4
3a(-18.5),Cs
$H_2C_3C_2C_1$=-89.8
3b(-15.9),Cs
4a(-16.6),Cs
4b(-16.4),Cs
4c(-14.6),Cs
4d(-13.4),Cs
5a(-13.4),Cs
5b(-11.4),Cs
6(-5.6),Cs
7(5.1),Cs
$H_1C_1C_2O$=-123.5
8a(27.6),Cs
8b(33.1),Cs
8c(29.9),C_1
$OC_1C_2C_3$=-147.8
$H_1OC_1C_2$=-6.3
$H_2C_2C_1C_3$=164.4
$H_3C_1C_2C_3$=23.8
8d(33.6),Cs
8e(31.1),C_1
$OC_1C_2C_3$=145.8
$H_1OC_1C_2$=-173.3
$H_2C_2C_1O$=-17.7
$H_3C_1C_2C_3$=-25.1

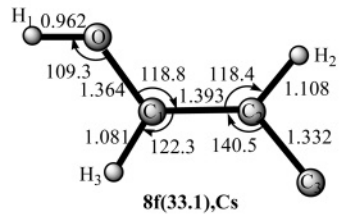

8f(33.1),Cs

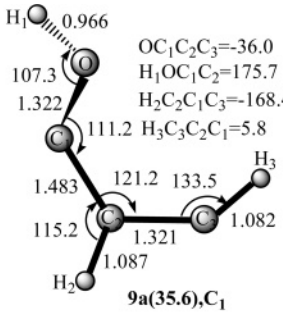

9a(35.6),C1

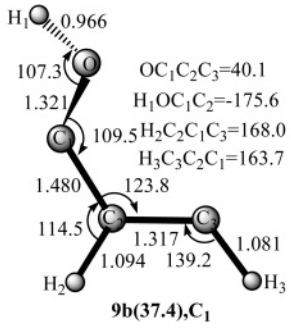

9b(37.4),C1

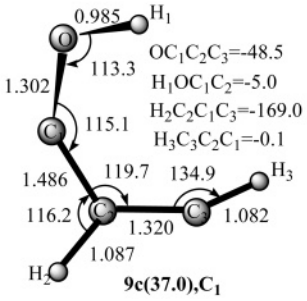

9c(37.0),C1

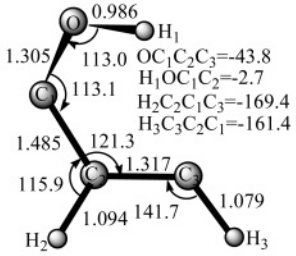

9d(37.7),C1

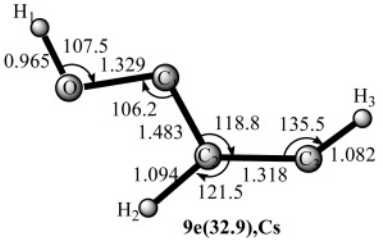

9e(32.9),Cs

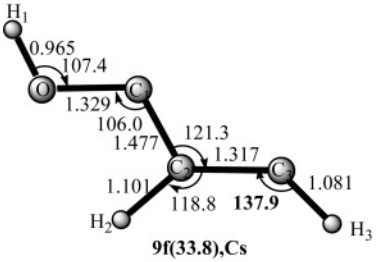

9f(33.8),Cs

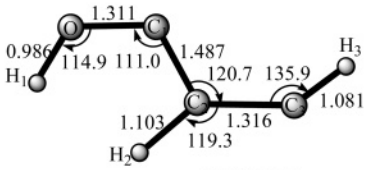

9g(36.2),Cs

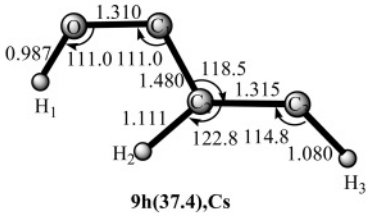

9h(37.4),Cs

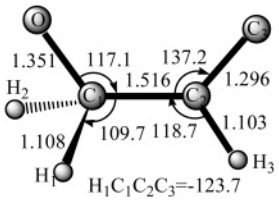

10(50.0),Cs

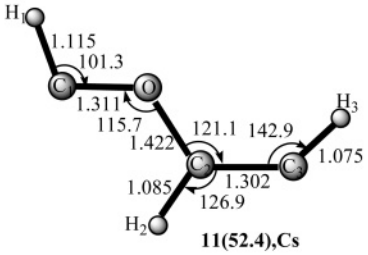

11(52.4),Cs

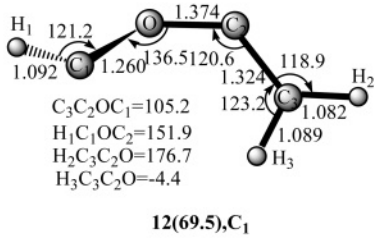

12(69.5),C1

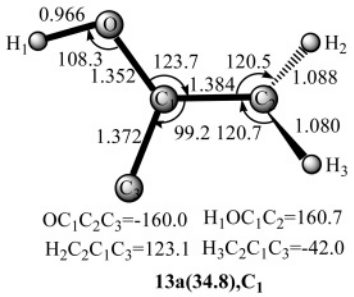

13a(34.8),C1

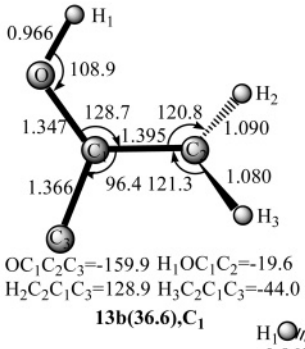

13b(36.6),C1

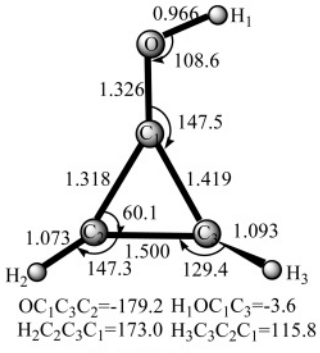

14a(16.0),C1

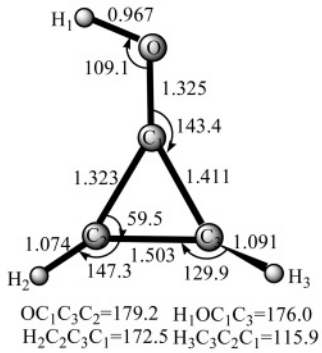

14b(16.4),C1

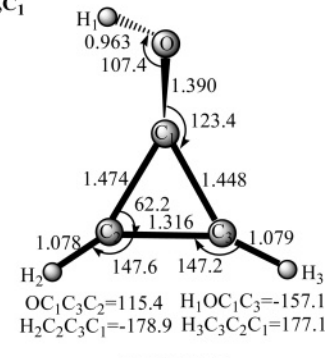

14c(18.8),C1

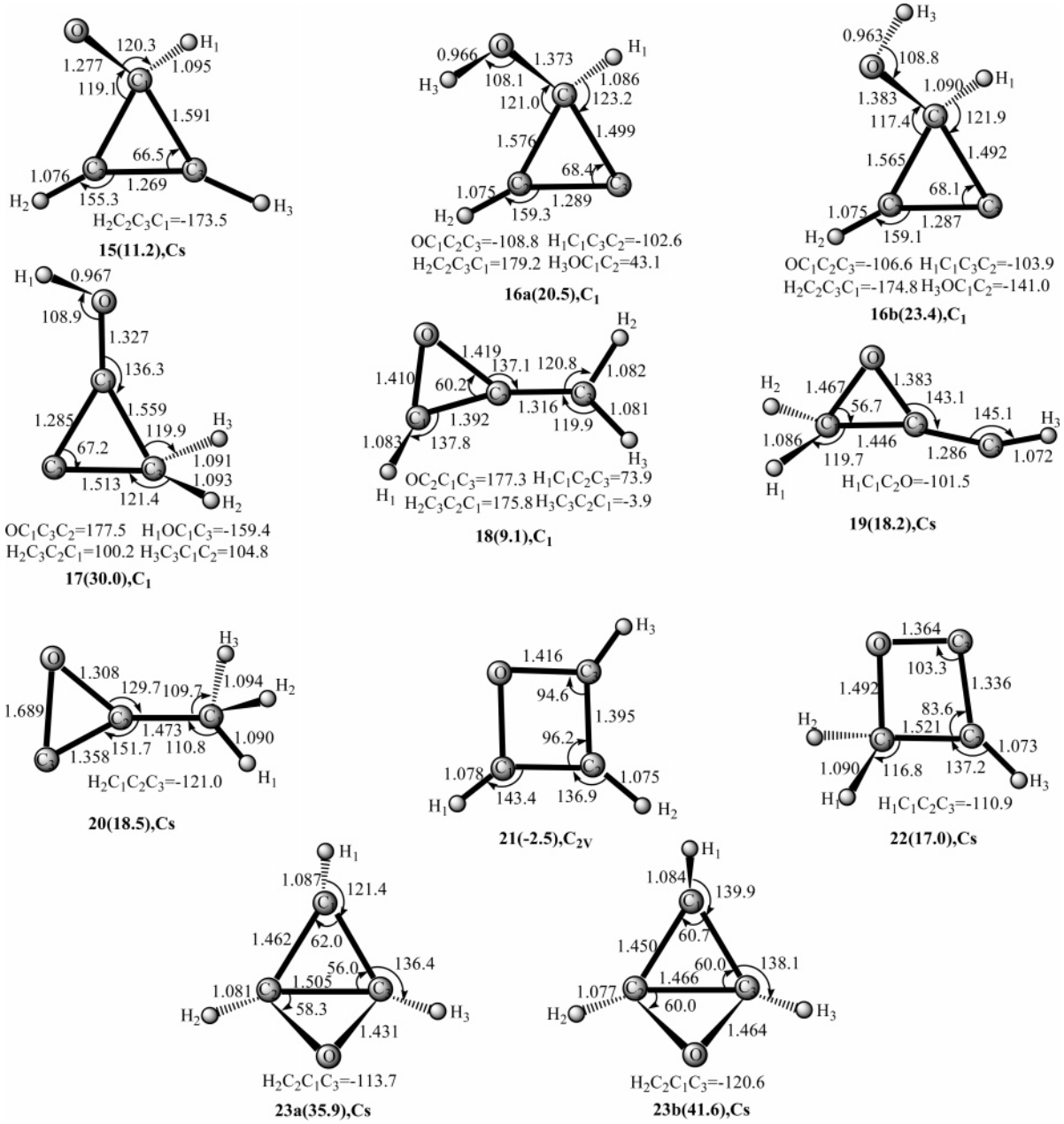

Figure 2. Optimized structures of isomers at B3LYP/6-311G(d,p) levels. Bond lengths are in angstroms and angles are in degrees.

3, is the direct C−H rupture to $\mathbf{P_3}$ HCCCHO + H (20.1) via **TS4a/P$_3$** (25.8). Though **TS4c/21** (26.0) of channel 4 is almost isoenergetic to **TS4a/P$_3$** of channel 3, the former channel should be less important than the latter because the four-membered-ring isomer *c*-CHCHCHO **21** (−2.5) would rather take a back-conversion to **4** than conversion to the high-energy *c*-CHCHCHO **23a** (35.9) with C−C cross-bonding. The channels 6, 7, and 8 forming H_2CCCHO **3a** (−18.5), $HCCCH_2O$ **7**, and HCCCHOH **5a** (47.2) are kinetically much less competitive than channel 2. Surely, the last channel (9) leading to the high-energy CHCHCOH **9a** (35.6) has negligible competition.

For the isomer H_2CCHCO **1** that is most favorably generated from **4a**, the direct C−C rupture leading to $\mathbf{P_1}$ C_2H_3 + CO via **TS1a/P$_1$** (−20.3) is the most feasible. The two transition states **TS1b/2** (12.5) and **TS1b/3a** (13.0) with comparable energies are associated with the corresponding conversion to the isomers H_3CCCO **2** (−27.3) and **3**. Surely, the large energy difference of 33 kcal/mol between **TS1a/P$_1$** and **TS1b/2**/**TS1b/3a** makes the **1b** → **2** and **1b** → **3a** conversions minutely competitive with **1a** → $\mathbf{P_1}$. The further transformations of **2** and **3** are not considered.

In a word, the former low-lying reaction pathways for the HCO + H_2CO reaction can be summarized as the following:

path 1: $\mathbf{R_1}$ HCO + C_2H_2 → HCCHCHO **4** →
H_2CCHCO **1** → $\mathbf{P_1}$ C_2H_3 + CO

path 2: $\mathbf{R_1}$ HCO + C_2H_2 → HCO···HCCH **Com1** →
$\mathbf{P_1}$ C_2H_3 + CO

path 3: $\mathbf{R_1}$ HCO + C_2H_2 → HCCHCHO **4** →
H_2CCHCO **1** → $\mathbf{P_3}$ HCCCHO + H

The overall barriers for the three pathways are 13.8 (**TS1a/4a**), 14.0 (**TSCom1/P$_1$**), and 25.8 (**TS4a/P$_3$**) kcal/mol, respectively, at the CCSD(T)//B3LYP level. Path 3 leading to propynal

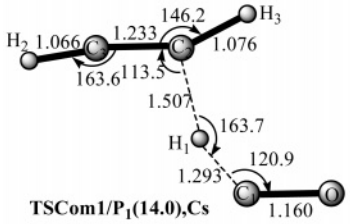

TSCom1/P$_1$(14.0),Cs

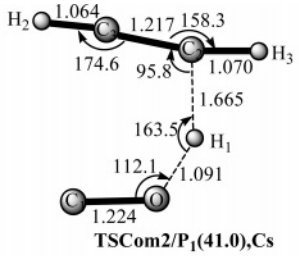

TSCom2/P$_1$(41.0),Cs

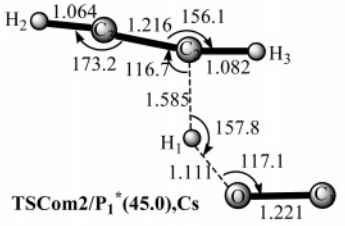

TSCom2/P$_1$*(45.0),Cs

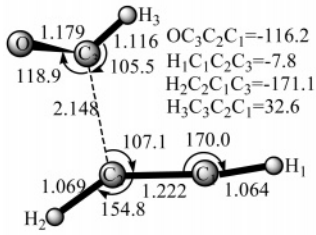

TSR$_1$/4b(10.5),C$_1$

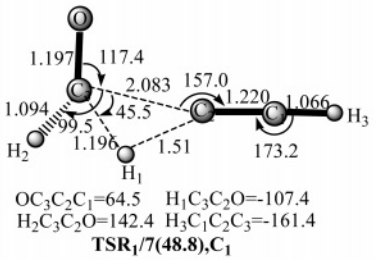

TSR$_1$/7(48.8),C$_1$

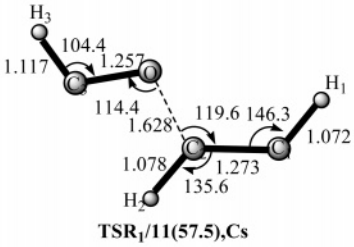

TSR$_1$/11(57.5),Cs

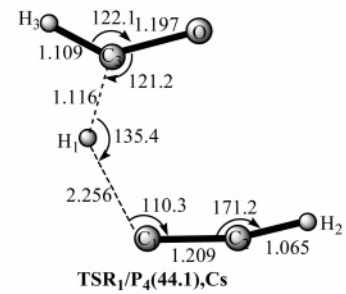

TSR$_1$/P$_4$(44.1),Cs

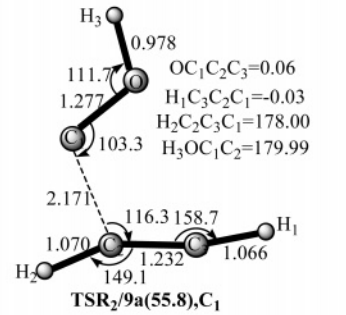

TSR$_2$/9a(55.8),C$_1$

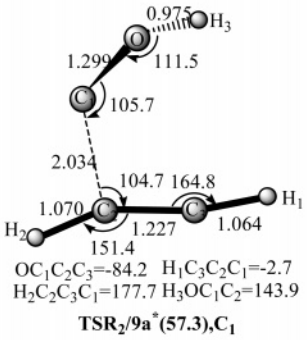

TSR$_2$/9a*(57.3),C$_1$

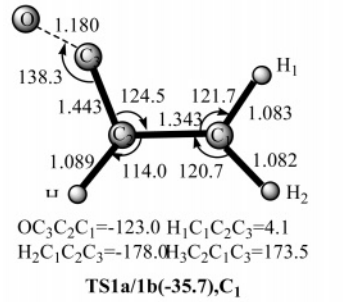

TS1a/1b(-35.7),C$_1$

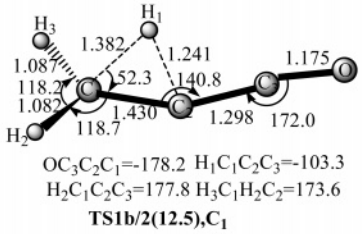

TS1b/2(12.5),C$_1$

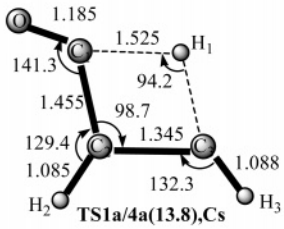

TS1a/4a(13.8),Cs

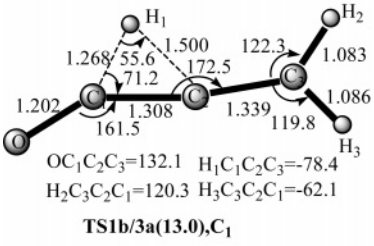

TS1b/3a(13.0),C$_1$

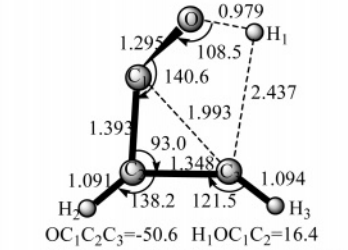

TS1a/14c(53.2),C$_1$

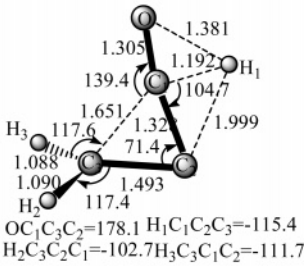

TS1b/17(85.4),C$_1$

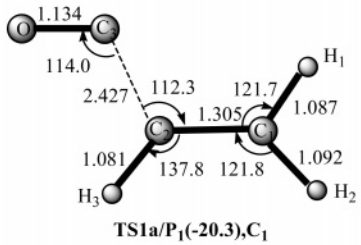

TS1a/P$_1$(-20.3),C$_1$

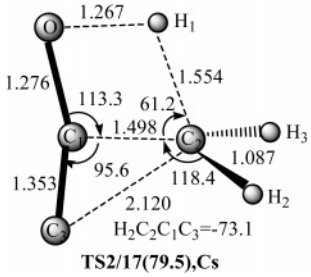

TS2/17(79.5),Cs

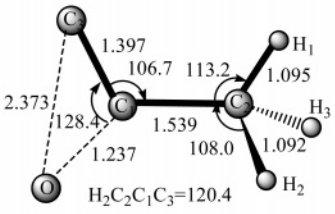

TS2/20(28.2),Cs

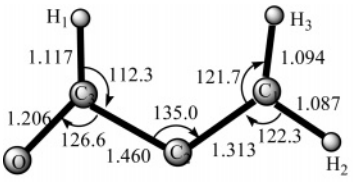

$OC_3C_2C_1$=160.0 $H_1C_3C_2C_1$=-20.5
$H_2C_1C_2C_3$=179.0 $H_3C_1C_2C_3$=-2.1

TS3a/3b(-15.8),22.9

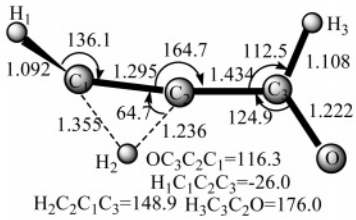

$OC_3C_2C_1$=116.3
$H_1C_1C_2C_3$=-26.0
$H_2C_2C_1C_3$=148.9 $H_3C_3C_2O$=176.0

TS3a/4b(31.7),C_1

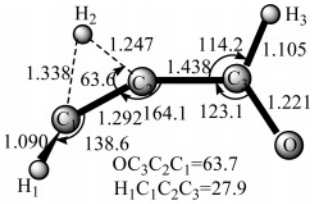

$OC_3C_2C_1$=63.7
$H_1C_1C_2C_3$=27.9
$H_2C_2C_1C_3$=-157.9 $H_3C_3C_2O$=176.0

TS3a/4c(31.6),C_1

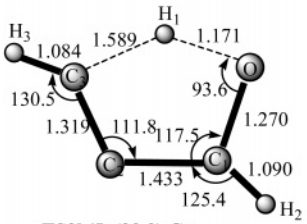

TS3b/5a(29.9),Cs

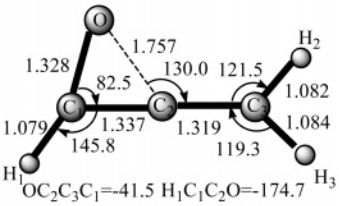

$OC_2C_3C_1$=-41.5 $H_1C_1C_2O$=-174.7
$H_2C_3C_2C_1$=61.0 $H_3C_3H_2C_1$=-120.2

TS3a/18(19.1),C_1

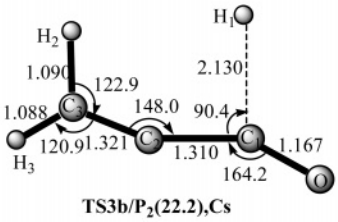

TS3b/P_2(22.2),Cs

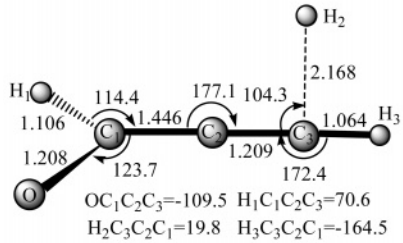

$OC_1C_2C_3$=-109.5 $H_1C_1C_2C_3$=70.6
$H_2C_3C_2C_1$=19.8 $H_3C_3C_2C_1$=-164.5

TS3a/P_3(22.4),C_1

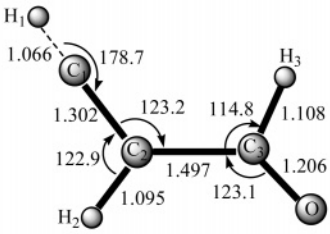

TS4a/4b(-12.5),Cs

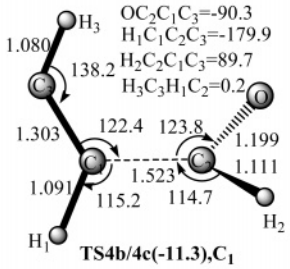

TS4b/4c(-11.3),C_1

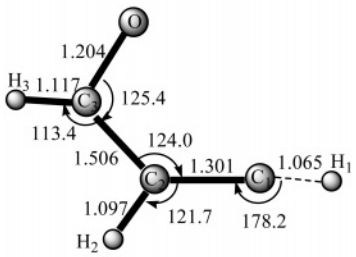

TS4c/4d(-9.7),Cs

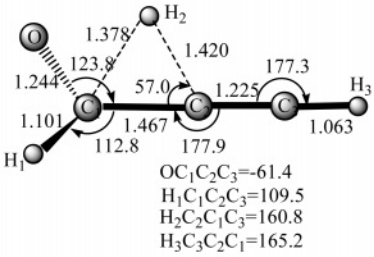

$OC_1C_2C_3$=-61.4
$H_1C_1C_2C_3$=109.5
$H_2C_2C_1C_3$=160.8
$H_3C_3C_2C_1$=165.2

TS4a/7(33.7),C_1

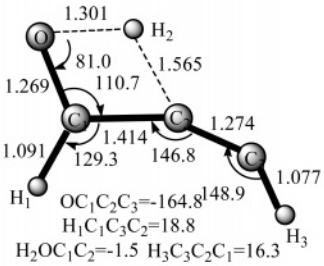

$OC_1C_2C_3$=-164.8
$H_1C_1C_3C_2$=18.8
$H_2OC_1C_2$=-1.5 $H_3C_3C_2C_1$=16.3

TS4b/5a(47.2),C_1

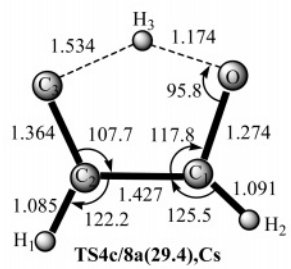

TS4c/8a(29.4),Cs

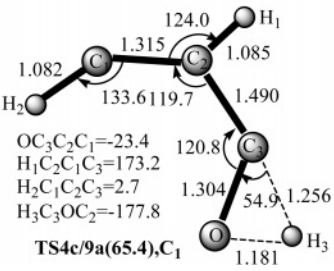

$OC_3C_2C_1$=-23.4
$H_1C_2C_1C_3$=173.2
$H_2C_1C_2C_3$=2.7
$H_3C_3OC_2$=-177.8

TS4c/9a(65.4),C_1

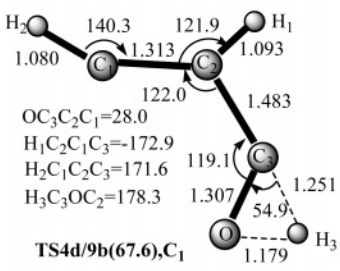

$OC_3C_2C_1$=28.0
$H_1C_2C_1C_3$=-172.9
$H_2C_1C_2C_3$=171.6
$H_3C_3OC_2$=178.3

TS4d/9b(67.6),C_1

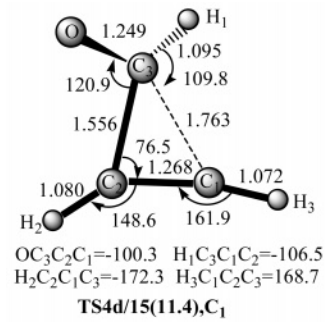

TS4d/15(11.4),C_1

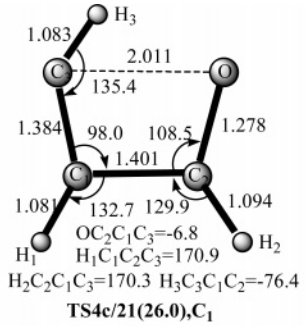

TS4c/21(26.0),C_1

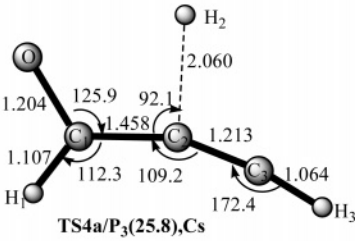

TS4a/P_3(25.8),Cs

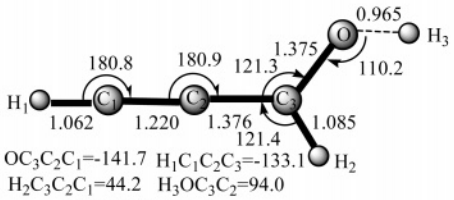

TS5a/5b(-8.3),C_1

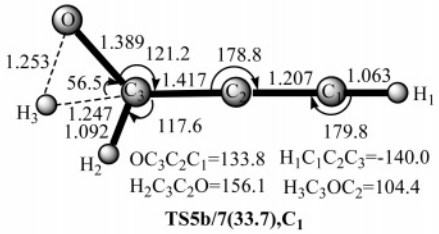

TS5b/7(33.7),C_1

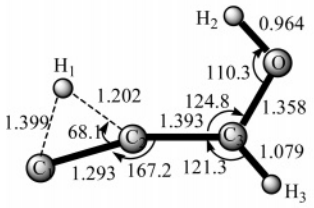

TS5a/8d(34.1),C_1

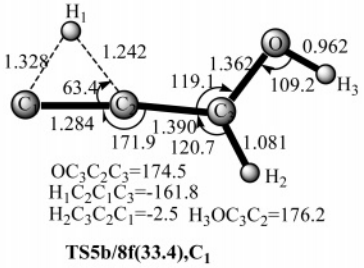

TS5b/8f(33.4),C_1

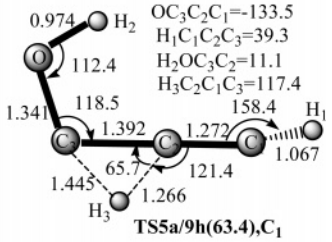

TS5a/9h(63.4),C_1

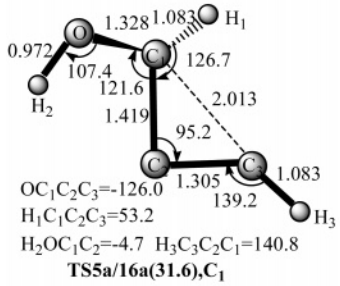

TS5a/16a(31.6),C_1

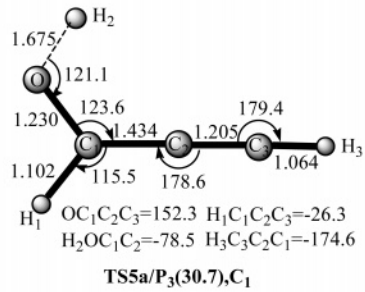

TS5a/P_3(30.7),C_1

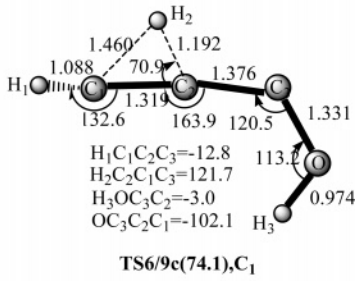

TS6/9c(74.1),C_1

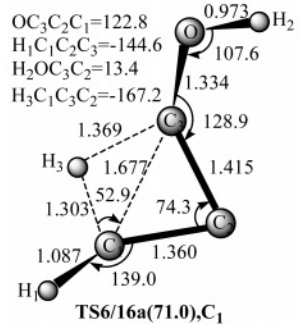

TS6/16a(71.0),C_1

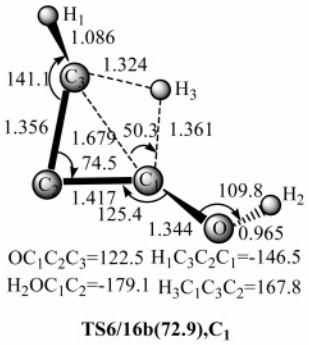

TS6/16b(72.9),C_1

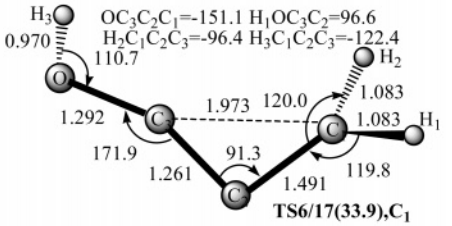

TS6/17(33.9),C_1

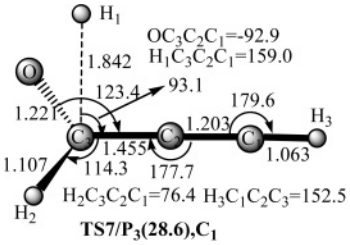

TS7/P_3(28.6),C_1

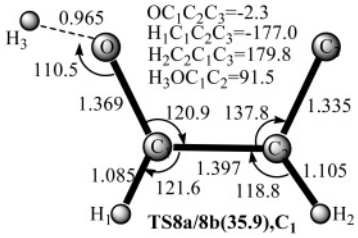

TS8a/8b(35.9),C_1

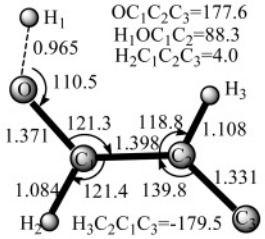

TS8c/8e(37.1),C_1

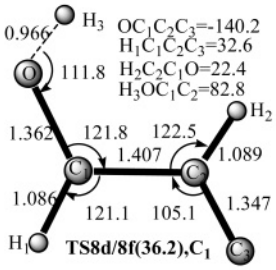

TS8d/8f(36.2),C_1

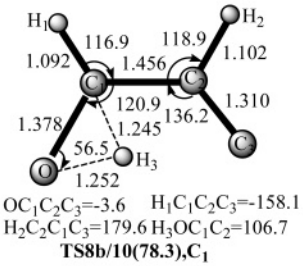

TS8b/10(78.3),C_1

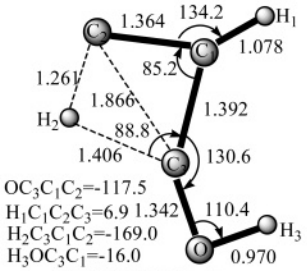

TS8d/14c(52.2),C_1

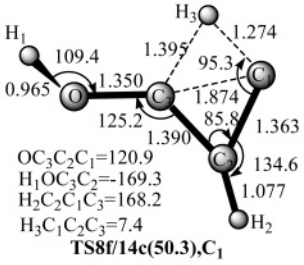

TS8f/14c(50.3),C_1

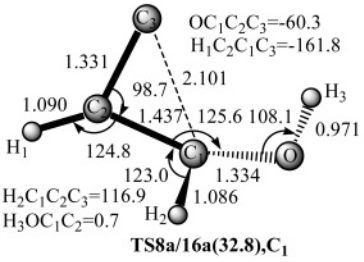

TS8a/16a(32.8),C_1

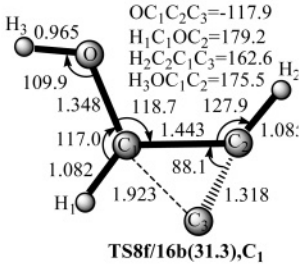

TS8f/16b(31.3),C_1

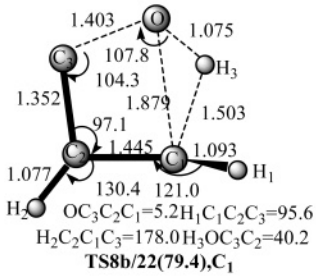

TS8b/22(79.4),C_1

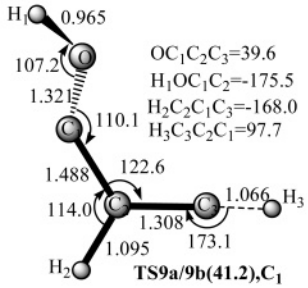

TS9a/9b(41.2),C_1

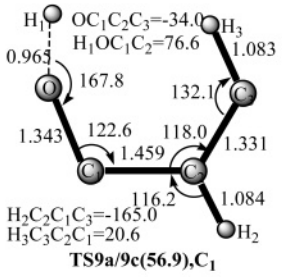

TS9a/9c(56.9),C_1

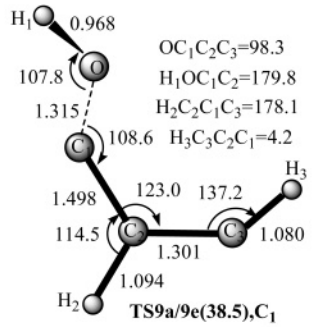

TS9a/9e(38.5),C_1

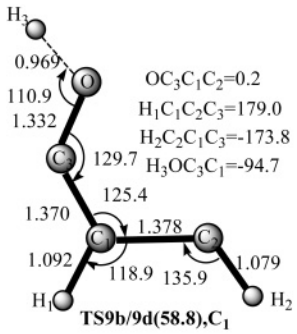

TS9b/9d(58.8),C_1

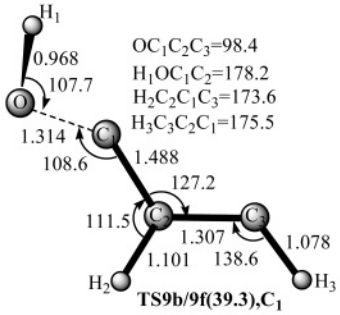

TS9b/9f(39.3),C_1

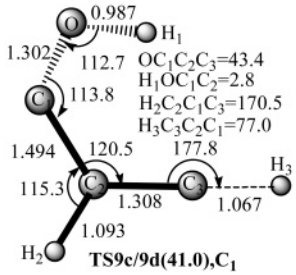

TS9c/9d(41.0),C_1

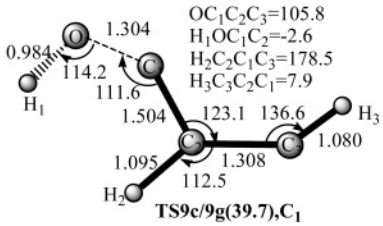

TS9c/9g(39.7),C_1

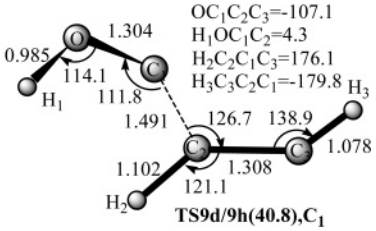

TS9d/9h(40.8),C_1

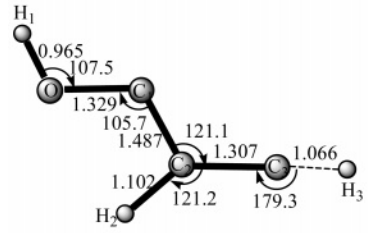

TS9e/9f(38.3),Cs

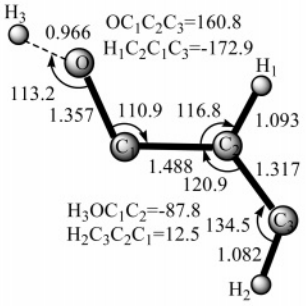

TS9e/9g(58.2),C1

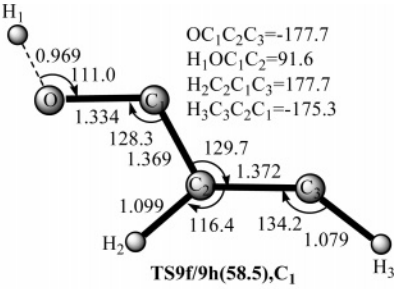

TS9f/9h(58.5),C1

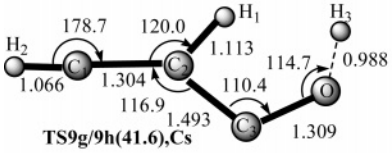

TS9g/9h(41.6),Cs

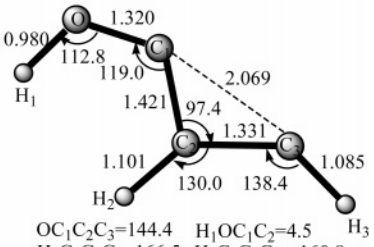

TS9h/14c(46.3),C1

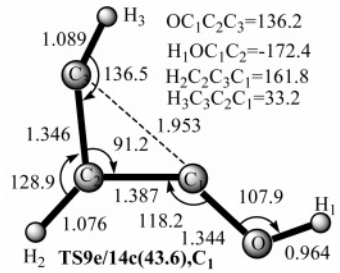

TS9e/14c(43.6),C1

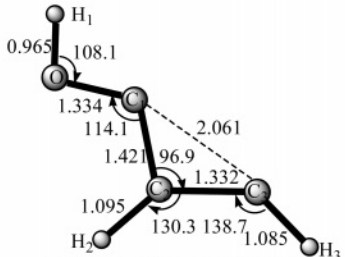

TS9f/14c(42.6),C1

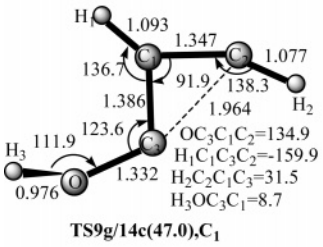

TS9g/14c(47.0),C1

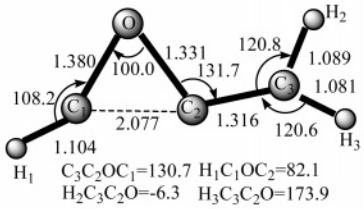

TS12/18(75.1),C1

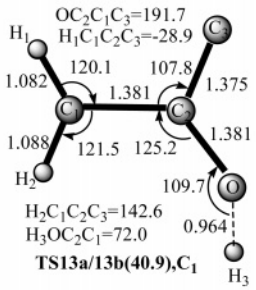

TS13a/13b(40.9),C1

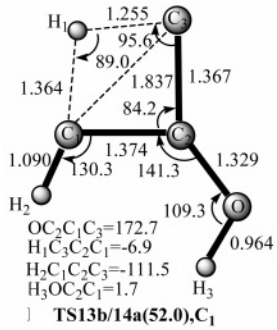

TS13b/14a(52.0),C1

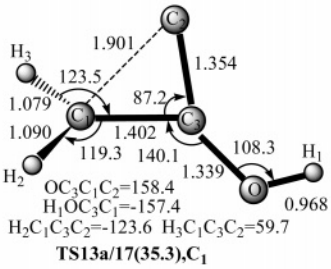

TS13a/17(35.3),C1

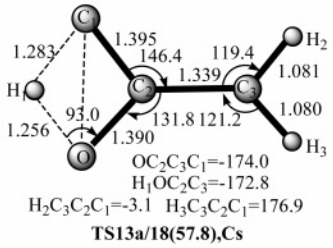

TS13a/18(57.8),Cs

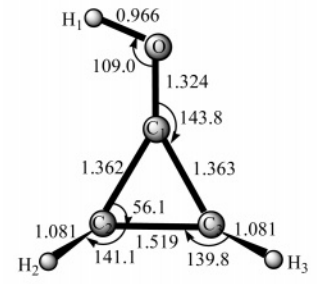

TS14a/14b(17.3),C1

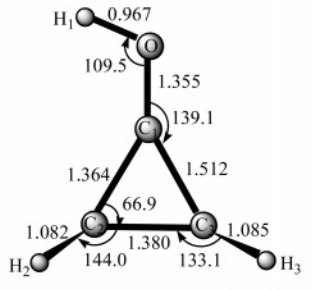

TS14b/14c(28.3),C1

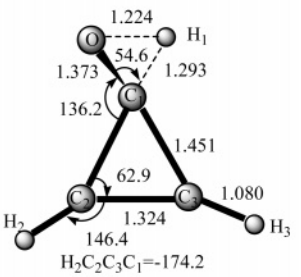

TS14c/15(54.3),Cs

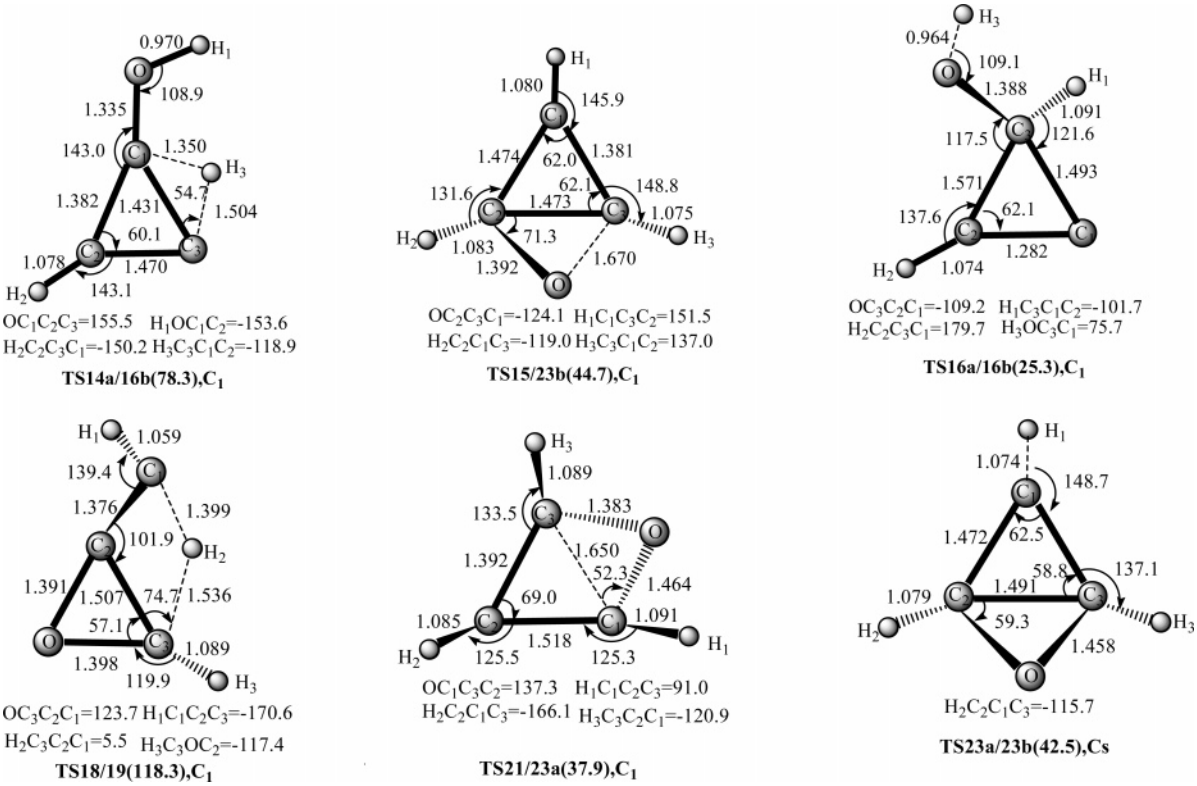

Figure 3. Optimized structures of interconversion transition states for the title reaction at B3LYP/6-311G(d,p) levels. Bond lengths are in angstroms and angles are in degrees.

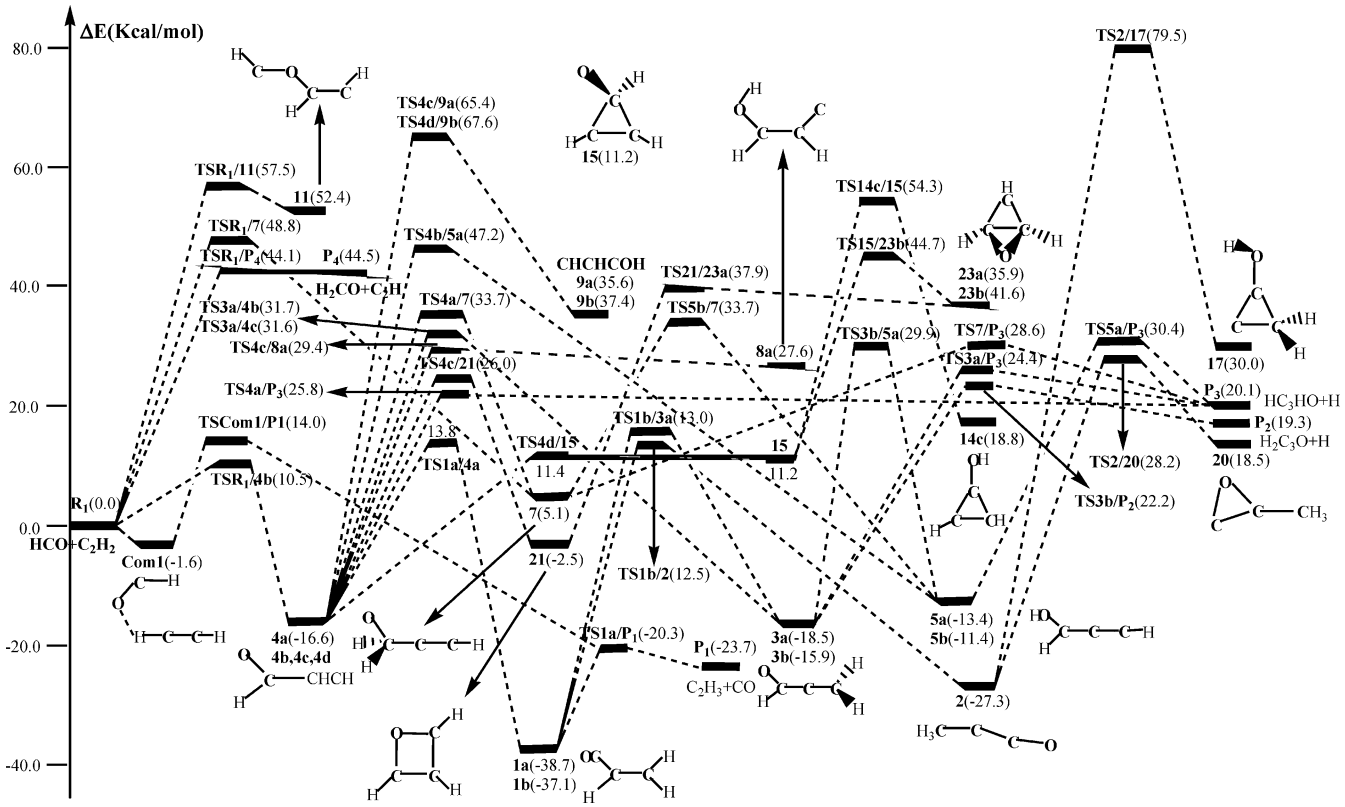

Figure 4. Schematic potential energy surface of HCO + C_2H_2 reaction at CCSD(T)/6-311G(2d,p)//B3LYP/6-311G(d,p)+ZPVE level.

HC≡CCH═O cannot compete with paths 1 and 2. At the higher G3//B3LYP and G3//MP2 levels, the corresponding relative energies are lowered to be 10.5 and 11.3 kcal/mol for **TS1a/4a** and 14.1 and 14.1 kcal/mol for **TSCom1/P1**. We conclude that path 1 is slightly more competitive than path 2. Both pathways lead to the same product **P1** C_2H_3 + CO. Also, the lowest energy pathway for propadiene $H_2C{=}C{=}C{=}O$ can be written as **R1** HCO + C_2H_2 → HCCHCHO **4** → H_2CCHCO **1** → H_2CCCHO **3** → **P2** H_2CCCO + H. Its competition is negligible. In fact, formation of propynal and propadiene is already thermodynami-

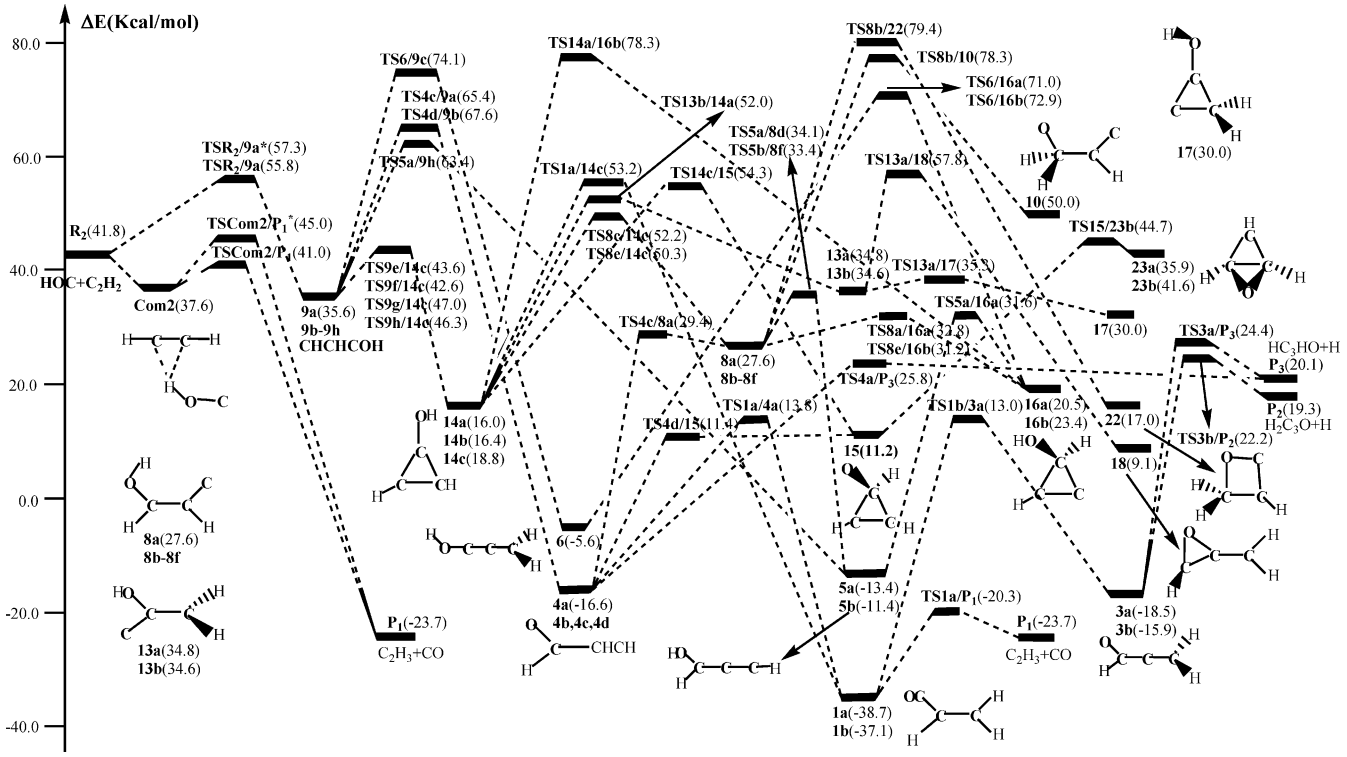

Figure 5. Schematic potential energy surface of HOC + C_2H_2 reaction at CCSD(T)/6-311G(2d,p)//B3LYP/6-311G(d,p)+ZPVE level.

cally unfavorable because **P₂** H_2CCCO + H (19.3) and **P₃** HCCCHO + H (20.1) each lie about 20 kcal/mol above **R₁**.

3.2. HOC + C_2H_2 Reaction. This reaction has never been studied. We first consider the entrance channels from **R₂** HOC + C_2H_2 (41.8) at the CCSD(T)//B3LYP level. The direct H-abstraction from C_2H_2 is not considered because the product **P₅** HCOH + C_2H (96.8) lies too much higher than **R₂**. As shown in Figure 5, the lowest lying channel is the quasi-direct H-donation leading to **P₁** C_2H_3 + CO (−23.7) via a prereactive complex COH···HCCH **Com2** (37.6). The lowered energy (−4.2) of **Com2** relative to **R₂** is more than that (−1.6) of **Com1** relative to **R₁**. This is due to the stronger OH···C_2 hydrogen bonding within **Com2**. The H-atom interacts with two C-atoms. Interestingly, there are two H-donation transition states connecting **Com2** and **P₁**, namely *cis*-**TSCom2/P₁** (41.0) and *trans*-**TSCom2/P₁*** (45.0). The latter lies 3.2 kcal/mol above **R₂**, whereas the former lies 0.8 kcal/mol lower than **R₂**. Higher level G3//B3LYP and G3//MP2 calculations predict *trans*-**TSCom2/P₁*** to lie 2.0 and 2.7 kcal/mol above **R₂**, and *cis*-**TSCom2/P₁** to be 1.9 and 1.1 kcal/mol lower than **R₂**. Clearly, at various levels, the H-donation channel via the lower energy transition state is barrierless. This is in sharp contrast to the HCO + C_2H_2 reaction, which has the H-donation barrier of 14.0 kcal/mol at the same level. Two factors contribute to this discrepancy: (1) the H−O bond in HOC is weaker than the H−C bond in HCO and (2) the formed prereactive species **Com2** is relatively more stable than **Com1**.

The other entrance channel is the direct C-addition leading to HOCCHCH **9** via **TSR₂/9a** (55.8) and **TSR₂/9a*** (57.3). Because both transition states are about 15 kcal/mol higher than **R₂**, this channel cannot compete with the H-donation channel and may be possible at high temperatures.

Isomer HOCCHCH **9** has eight isomeric forms **9a**−**9h** with easy interconversion among one another. In addition to back-dissociation to **R₂**, there are four types of conversion pathways: **9** → **14**, **9** → **5**, **9** → **4**, and **9** → **6**. The latter three pathways have much lower energy isomers, HCCCHOH **5a** (−13.4)/**5b** (−11.4), HCCHCHO **4a** (−16.6)/**4b** (−16.4)/**4c** (−14.6)/**4d** (−13.4), and H_2CCCOH **6** (−5.6), than the first ring-closure pathway, leading to the three-membered-ring isomers **14a** (16.0), **14b** (16.4), and **14c** (18.8). However, the first pathway is kinetically much more favorable by about 20 kcal/mol. Thus we focus on the **9** → **14** conversion. Starting from **14**, there are four conversion channels: **14** → **8**, **14** → **13**, **14** → **15**, **14** → **1**, and **14** → **16**. Because of the rather high energy of **TS14a/16b** (78.3), the last channel leading to the ring isomer HO-*c*-CHCCH **16a** (20.5)/16b (23.4) is excluded. The remaining channels have close energy transition states as **TS8e/14c** (50.3)/**TS8c/14c** (52.2), **TS13b/14a** (52.0), **TS1a/14c** (53.2), and **TS14c/15** (54.3). For channel **14** → **13**, the formed isomer **13a** (34.8)/**13b** (34.6) can very easily isomerize to **17** (30.0). Yet further, the lowest evolution of **17** is conversion to **13** and to **14**. Therefore, we also exclude this channel. Now we write the further most feasible isomerization pathways after the **14** → **8**, **14** → **15**, and **14** → **1** channels: **8** → **4** → **1** → **P₁** C_2H_3 + CO, **15** → **4** → **1** → **P₁** C_2H_3 + CO, and **1** → **P₁** C_2H_3 + CO, respectively. Thus, the most favorable product via the C-addition is also the low-lying product **P₁** C_2H_3 + CO.

Different from the HCO + C_2H_2 reaction, formation of propadiene and propynal is thermodynamically accessible because **P₂** H_2CCCO + H and **P₃** HCCCCHO + H are 22.5 and 20.7 kcal/mol lower than **R₂** HOC + C_2H_2. They have to be formed via the C-addition channels:

R₂ HOC + C_2H_2 → **9** → **14** → **8** → **4** → **1** → **3** → **P₂** H_2CCCO + H

R₂ HOC + C_2H_2 → **9** → **14** → **8** → **4** → **P₃** HCCCCHO + H

Surely, both cannot compete with the **P₁** C_2H_3 + CO-formation channel:

$$\mathbf{R_2}\ HOC + C_2H_2 \rightarrow \mathbf{9} \rightarrow \mathbf{14} \rightarrow \mathbf{8} \rightarrow \mathbf{4} \rightarrow \mathbf{1} \rightarrow \mathbf{P_1}\ C_2H_3 + CO$$

3.3. Combustion and Interstellar Implications. Both HCO/HOC + C_2H_2 reactions have not been previously studied. For the HCO reaction, both the most feasible C-addition channel and the slightly less competitive H-donation channel lead to $\mathbf{P_1}$ C_2H_3 + CO. With the considerable entrance barriers (around 10 kcal/mol), this reaction cannot take place at low temperatures. Yet it is feasible at higher temperatures. In the postcombustion regions of acetylene, it could play a role. In contrast, the HOC reaction can take a barrierless H-donation process leading to $\mathbf{P_1}$ C_2H_3 + CO. This indicates that this reaction may easily take place even at low temperatures. This is particularly attractive in dense molecular clouds where the temperature is less than 100 K. We should note that the present paper represents the first consideration of the HOC reactions.

4. Conclusions

A detailed theoretical study is carried out for the unknown HCO/HCO + C_2H_2 reactions at the CCSD(T)/6-311G(2d,p)//B3LYP/6-311G(d,p)+ZPVE, Gaussian-3//B3LYP/6-31G(d), and Gaussian-3//MP2(full)/6-31G(d) levels. For the HCO + C_2H_2 reaction, both the most feasible C-addition channel and the slightly less competitive H-donation channel lead to $\mathbf{P_1}$ C_2H_3 + CO. With the considerable entrance barriers (around 10 kcal/mol), this reaction cannot take place at low temperatures. Yet it is feasible at higher temperatures. In the postcombustion regions of acetylene, it could play a role. In contrast, the HOC + C_2H_2 reaction can take a barrierless H-donation process leading to $\mathbf{P_1}$ C_2H_3 + CO. This indicates that this reaction may easily take place even at low temperatures. This is particularly attractive in dense molecular clouds where the temperature is less than 100 K. The weak H−O bond in HOC and the ability to form a hydrogen-bonded complex with π-systems can provide effective means to deplete the HOC radical. The present paper represents the first consideration of the HOC reactions.

Acknowledgment. This work was supported by the National Natural Science Foundation of China (20103003), the Doctor Foundation of Educational Ministry, and the Excellent Young Teacher Foundation of Ministry of Education of China.

References and Notes

(1) Pauzat, F.; Chekir, S.; Ellinger, Y. *J. Chem. Phys.* **1986**, *85*, 2861, and references therein.
(2) Hasegawa, T. I.; Herbst, E. *Mon. Not. R. Astron. Soc.* **1993**, *263*, 589.
(3) Dunning, T. H., Jr. *J. Chem. Phys.* **1980**, *73*, 2304.
(4) Bowman, J. M. Bittman, J. S. Harding, L. B. *J. Chem. Phys.* **1986**, *85*, 911.
(5) Peric, M.; Marian, C. M.; Peyerimhoff, S. D. *J. Mol. Spectrosc.* **1994**, *166*, 406.
(6) Staikova, M.; Peric, M.; Engels, B.; Peyerimhoff, S. D. *J. Mol. Spectrosc.* **1994**, *166*, 423.
(7) Serano-Andres, L.; Forsberg, N.; Malmqvist, P.-A. *J. Chem. Phys.* **1998**, *108*, 7202.
(8) Mourik, T. V.; Dunning, T. H., Jr.; Peterson, K. A. *J. Phys. Chem. A* **2000**, *104*, 2287.
(9) Friedrichs, G.; Herbon, J. T.; Davidson, D. F.; Hanson, R. K. *Phys. Chem. Chem. Phys.* **2002**, *4*, 5778, and references therein.
(10) Dixon, D. A.; Feller, D.; Francisco, J. S. *J. Phys. Chem. A* **2003**, *107*, 186.
(11) Marenich, A. V.; Boggs, J. E. *J. Phys. Chem. A* **2003**, *107*, 2343.
(12) Yeom, Y. H.; Frei, H. *J. Phys. Chem. B* **2003**, *107*, 6286.
(13) Marenich, A. V.; Boggs, J. E. *J. Phys. Chem. A* **2004**, *108*, 5431.
(14) Hippler, H.; Krasteva, N.; Striebel, F. *Phys. Chem. Chem. Phys.* **2004**, *6*, 3383.
(15) Krasnoperov, L. N.; Chesnokov, E. N.; Stark, H.; Ravishankara, A. R. *J. Phys. Chem. A* **2004**, *108*, 11526.
(16) Hochanadel, C. J.; Sworskl, T. J.; Ogren, P. J. *J. Phys. Chem.* **1980**, *84*, 231.
(17) Butkovskaya, N. I.; Setser, D. W. *J. Phys. Chem. A* **1998**, *102*, 9715.
(18) Qu, Z.; Dong, F.; Zhang, Q.; Kong, F. *Chem. Phys. Lett.* **2004**, *386*, 384.
(19) Becerra, B.; Carpenter, I. W.; Walsh, R. *J. Phys. Chem. A* **1997**, *101*, 4185.
(20) Veyret, B.; Lesclaux, R. *J. Phys. Chem.* **1981**, *85*, 1918.
(21) Timonen, R. S.; Ratajczak, R.; Gutman, D. *J. Phys. Chem.* **1988**, *92*, 651.
(22) Nesbitt, F. L. *J. Phys. Chem. A* **1999**, *103*, 3038.
(23) Yamasaki, K.; Sato, M.; Itakura, A.; Watanabe, A.; Kakuda, T.; Tokue, I. *J. Phys. Chem. A* **2000**, *104*, 6517.
(24) Ninomiya, Y.; Goto, M.; Hashimoto, S.; Kagawa, Y.; Yoshizawa, K.; Kawasaki, M.; Wallington, T. J.; Hurley, M. D. *J. Phys. Chem. A* **2000**, *104*, 7556.
(25) Hanoune, B.; Dusanter, S.; ElMaimouni, L.; Devolder, P.; Lemoine, B. *Chem. Phys. Lett.* **2001**, *343*, 527.
(26) DeSain, J. D.; Jusinski, L. E.; Ho, A. D.; Taatjes, C. A. *Chem. Phys. Lett.* **2001**, *347*, 79.
(27) Martinez-Avila, M.; Peiro-Garcia, J.; Ramirez-Ramirez, V. M.; Nebot-Gil, I. *Chem. Phys. Lett.* **2003**, *370*, 313.
(28) Kulkarni, S. A.; Koga, N. *J. Phys. Chem. A* **1998**, *102*, 5228.
(29) Yarwood, G.; Niki, H.; Maker, P. D. *J. Phys. Chem.* **1991**, *95*, 4773.
(30) Feng, W. L.; Wang, Y.; Zhang, S. W.; Pang, X. Y. *Chem. Phys. Lett.* **1997**, *266*, 43.
(31) Xu, Z. F.; Lin, M. C. *Int. J. Chem. Kinet.* **2004**, *36*, 205.
(32) Guo, Y.; Smith, S. C.; Moore, C. B.; Melius, C. F. *J. Phys. Chem.* **1995**, *99*, 7473.
(33) Rim, K. T.; Hershberger, J. F. *J. Phys. Chem. A* **1998**, *102*, 5898.
(34) Meyer, St.; Temps, F. *Int. J. Chem. Kinet.* **2000**, *32*, 136.
(35) Zhang, X. H.; Xu, Z. F.; Ji, Y. Q.; Feng, W. L.; Lei, M. *Chin. J. Chem. Phys.* **2003**, *16*, 94.
(36) Xu, Z. F.; Lin, M. C. *Int. J. Chem. Kinet.* **2004**, *36*, 178.
(37) Baggott, J. E.; Frey, H. M. Lightfoot, P. D.; Walsh, R. *J. Phys. Chem.* **1987**, *91*, 3386, and references therein.
(38) Frisch, M. J.; Trucks, G. W.; Schlegel, H. B.; Scuseria, G. E.; Robb, M. A.; Cheeseman, J. R.; Zakrzewski, V. G.; Montgomery, J. A., Jr.; Stratmann, R. E.; Burant, J. C.; Dapprich, S.; Millam, J. M.; Daniels, A. D.; Kudin, K. N.; Strain, M. C.; Farkas, O.; Tomasi, J.; Barone, V.; Cossi, M.; Cammi, R.; Mennucci, B.; Pomelli, C.; Adamo, C.; Clifford, S.; Ochterski, J.; Petersson, G. A.; Ayala, P. Y.; Cui, Q.; Morokuma, K.; Malick, D. K.; Rabuck, A. D.; Raghavachari, K.; Foresman, J. B.; Cioslowski, J.; Ortiz, J. V.; Stefanov, B. B.; Liu, G.; Liashenko, A.; Piskorz, P.; Komaromi, I.; Gomperts, R.; Martin, R. L.; Fox, D. J.; Keith, T.; Al-Laham, M. A.; Peng, C. Y.; Nanayakkara, A.; Gonzalez, C.; Challacombe, M.; Gill, P. M. W.; Johnson, B. G.; Chen, W.; Wong, M. W.; Andres, J. L.; Head-Gordon, M.; Replogle, E. S.; Pople, J. A. *Gaussian 98*, revision A.11; Gaussian, Inc.: Pittsburgh, PA, 2001.
(39) Steudel, R. In *Chemistry of the Non-Metals*; Walter de Gruyter: Hawthorne, NY, 1977.